Journal of Geotechnical and Geoenvironmental Engineering, ASCE, Vol. 135, No. 10, pp. 1404-1418, 2009

On the influence of the grain size distribution curve of quartz sand on the small strain shear modulus $G_{\max}$

T. Wichtmann[i)], Th. Triantafyllidis[ii)]

Abstract: The paper presents a study of the influence of grain size distribution curve on the small strain shear modulus $G_{\max}$ of quartz sand with sub-angular grain shape. The results of 163 resonant column tests on 25 different grain size distribution curves are presented. It is demonstrated for a constant void ratio that while $G_{\max}$ is not influenced by variations in the mean grain size d_{50} in the investigated range, it significantly decreases with increasing coefficient of uniformity $C_u = d_{60}/d_{10}$ of the grain size distribution curve. Well-known empirical formulas (e.g. Hardin's equation with its commonly used constants) may strongly overestimate the stiffness of well-graded soils. Based on the RC test results, correlations of the constants of Hardin's equation with C_u have been developed. The predictions using Hardin's equation and these correlations are in good accordance with the test data. Correlations of the frequently used shear modulus coefficient $K_{2,\max}$ with C_u and empirical equations formulated in terms of relative density D_r, are also given in the paper. A comparison of the predictions by the proposed empirical formulas with $G_{\max}$-data from the literature and a micromechanical explanation of the experimental results are provided. Correction factors for an application of the laboratory data to in-situ conditions are also discussed.

CE Database subject headings: Small strain shear modulus; Quartz sand; Grain size distribution curve; Coefficient of uniformity; Resonant column tests;

Introduction

The resilient and the residual displacements of foundations under cyclic or dynamic loading are of interest in practice. The residual displacements are discussed in detail elsewhere (Niemunis et al. [36], Wichtmann [51], Wichtmann et al. [52, 53]). For small strain amplitudes ($\gamma < 0.005$ % for sand) residual deformations due to repeated load applications are negligible and the resilient behavior is of main concern. Soil behavior is adequately described by an elastic constitutive model. The secant shear stiffness $G_{\sec}$ of the shear stress-shear strain hysteresis is the most important design parameter for an analysis of the resilient displacements.

The secant shear stiffness $G_{\sec}$ decreases with increasing shear strain amplitude γ if a certain threshold value ($\gamma \approx 0.001$ % for sand) is surpassed. The maximum shear modulus at very small strain amplitudes is denoted as $G_{\max}$. It can be determined in situ from measurements of the shear wave velocity v_S where $G_{\max} = \varrho(v_S)^2$ with ϱ being the density of the soil. Measurements of the shear wave velocity in situ have become a commonplace tool for the design of foundations subjected to a repeated loading during recent years. Bore-hole methods (cross-hole, down-hole, up-hole) may be applied, as well as the seismic CPT or the analysis of a steady vibration applied at the surface. However, empirical formulas for $G_{\sec}$ or $G_{\max}$ may be beneficial for practical purpose in the following cases (Gazetas [16]):

- for feasibility studies and preliminary design calculations, before any in-situ or laboratory measurements have been performed
- for final design calculations in small projects where the costs of a proper testing for $G_{\max}$ are not justified (e.g. foundations of small on-shore wind power plants)
- to provide an order-of-magnitude check against experimentally determined values

Several such empirical formulas have been proposed in the literature. A multiplicative approach is usually applied for $G_{\sec}$:

$$G_{\sec} = G_{\max}(e,p)\ F(\gamma) \tag{1}$$

For a given sand, $G_{\max}$ is mainly a function of void ratio e and effective mean pressure p. $F(\gamma)$ is a function which describes the decrease of $G_{\sec}$ with increasing shear strain amplitude. It is equal to one for very small γ-values ($<$ 0.0001 %). Appropriate curves $F(\gamma)$ were proposed for example by Seed et al. [45].

A widely used empirical formula for the small strain shear modulus $G_{\max}(e,p)$ is one proposed by Hardin [17, 19]:

$$G_{\max} = A\ \frac{(a-e)^2}{1+e}\ p^n \tag{2}$$

with $G_{\max}$ in [MPa] and p in [kPa]. It was developed based on tests on Ottawa sand and on a crushed quartz sand. The constants $A = 6.9$, $a = 2.17$ and $n = 0.5$ for round grains, and $A = 3.2$, $a = 2.97$ and $n = 0.5$ for angular grains were recommended in [17] and are often used for estimations of $G_{\max}$-values for various sands.

Seed & Idriss [44] (see also Seed et al. [45]) proposed the simplified relationship (converted to SI units):

$$G_{\max} = 218.8\ K_{2,\max}\ p^{0.5} \tag{3}$$

[i)] Research Assistant, Institute of Soil Mechanics and Rock Mechanics, University of Karlsruhe, Germany (corresponding author). Email: torsten.wichtmann@ibf.uka.de

[ii)] Professor and Director of the Institute of Soil Mechanics and Rock Mechanics, University of Karlsruhe, Germany

with $G_{\max}$ and p in [kPa] and a dimensionless modulus coefficient $K_{2,\max}$. Eq. (3) is frequently used in the U.S. to estimate $G_{\max}$. Seed et al. [45] stated that $K_{2,\max}$-values obtained from laboratory tests range from about 30 for loose sands to about 75 for dense sands. For gravelly soils, somewhat higher values of $K_{2,\max}$ were measured.

Alternative equations (e.g. Roesler [41], Knox et al. [25], Bellotti et al. [7]) were formulated with the effective stress components σ_a and σ_p in the directions of the shear wave propagation and polarization, respectively, instead of p. However, Gazetas [16] stated that S-waves may propagate in all directions away from a dynamically loaded foundation. It may not be readily evident which are the a and b directions. Thus, the use of p may be as advantageous.

Eq. (2) with the given constants does not reflect the strong dependence of the small strain shear modulus on the grain size distribution curve, especially on the coefficient of uniformity $C_u = d_{60}/d_{10}$ and on the fines content. A respective literature review is given in the next section. It appears that an application of Eq. (2) to well-graded soils using the constants proposed by Hardin may strongly overestimate $G_{\max}$.

The present paper aims to contribute to a better fundamental understanding of the influence of the grain size distribution curve on $G_{\max}$. It reports on our effort to extend Eqs. (2) and (3) by the influence of the grain size distribution curve, in particular by the coefficient of uniformity C_u. 163 resonant column (RC) tests on 25 different grain size distribution curves have been performed for this purpose.

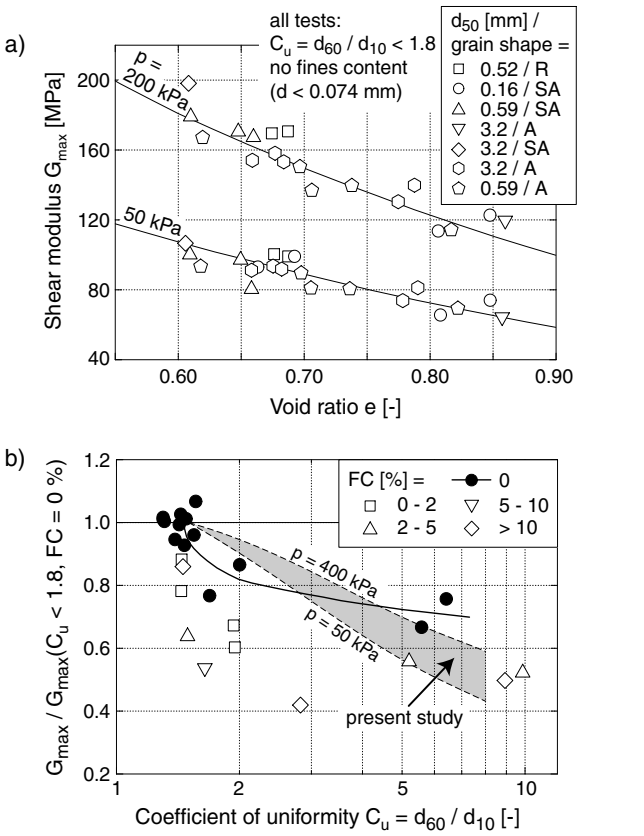

Fig. 1: a) No influence of d_{50} on $G_{\max}$ for poorly graded sands without a fines content (R: round grains, SA: subangular grains, A: angular grains), b) Decrease of $G_{\max}$ with increasing coefficient of uniformity C_u and with increasing fines content, test results of Iwasaki & Tatsuoka [23]

Literature review

Few recommendations are given in the literature on how to consider the influence of the grain size distribution curve when estimating $G_{\max}$ of sands or gravels.

Based on RC tests, Iwasaki & Tatsuoka [23] reported that for a constant void ratio $G_{\max}$ is strongly affected by the grain size distribution curve. For poorly graded sands ($C_u < 1.8$, 0.16 mm $\leq d_{50} \leq$ 3.2 mm) without a fines content (i.e. no grains smaller than $d = 0.074$ mm) the values of $G_{\max}(e)$ did not depend on d_{50} (Fig. 1a). Furthermore, Iwasaki & Tatsuoka [23] could not observe a significant influence of the grain shape (Fig. 1a). Similar $G_{\max}$-values were measured for sands with round, subangular and angular grains. Fig. 1b presents tests of Iwasaki & Tatsuoka [23] on grain size distribution curves with different coefficients of uniformity and different fines contents. The measured shear moduli $G_{\max}$ were normalized by the values of the poorly-graded sands without a fines content at same values of e and p . $G_{\max}$ decreases significantly with increasing C_u and with increasing FC. However, only one test was performed for most of the sands and Iwasaki & Tatsuoka [23] did not extend Eq. (2) by the influence of C_u or FC.

Edil & Luh [13] proposed a relationship $G_{\max}(d_{10}, d_{50}, C_u, e)$ for $p = 211$ kPa. However, evaluating this relationship for the sands used in the present study does not deliver meaningful results, for example for fine sands an increase of $G_{\max}$ with increasing e is predicted.

Rollins et al. [42] presented tests in which the content of gravel was increased from 0 % to 60 %. A simultaneous increase of the small strain shear modulus $G_{\max}$ by 38 % was observed. However, the C_u-values of the tested materials were not given in [42].

Menq & Stokoe [34] performed RC tests in order to measure the $G_{\max}$-values of ten grain size distribution curves of a natural river sand. The sands had different d_{50}- and C_u-values and did not contain fines. For each sand three different initial densities (loose, medium dense and dense) were studied. Relatively large specimen dimensions (sample diameter $d = 15$ cm, height $h = 30$ cm) were used. In contrast to Iwasaki & Tatsuoka [23], a slight increase of $G_{\max}$ with increasing d_{50} was measured for $e, p =$ constant. Furthermore, the curves of $G_{\max}(e)$ were steeper for the coarse material. For a constant relative density Menq & Stokoe [34] reported slightly higher $G_{\max}$-values for dense samples with $C_u \approx 10$ than for dense samples with $C_u \approx 1.2$, in other words $G_{\max}$ increases with C_u for $D_r =$ constant. Probably this is not in contrast to the test results of Iwasaki & Tatsuoka [23] since Menq & Stokoe [34] compared similar relative densities while Iwasaki & Tatsuoka [23] compared similar void ratios. Menq & Stokoe [34] also found that the exponent n in Eq. (2) increases with increasing C_u.

A study of Lontou & Nikolopoulou [32] with RC tests on natural sands containing approximately a single grain size showed a slight increase of $G_{\max}$ with the mean grain size up to $d_{50} = 1.8$ mm. Significantly higher values for $d_{50} > 1.8$ mm may be influenced by the small specimen size (diameter $d = 4.8$ cm).

Hardin & Kalinski [18] performed 17 RC tests on differ-

ent sands and sand-gravel mixtures. In the large-scale RC tests (sample dimensions $d = 15$ cm, $h = 30$ cm) on predominantly gravelly soils the lateral stress was applied by vacuum. The small-strain shear moduli of the gravels were found to be significantly larger than those of the uniform sands. Thus, $G_{\max}$ increased with increasing d_{50}. Hardin & Kalinski [18] proposed an extended equation, similar to (2), but containing a factor which is 1 for sand and which becomes > 1 for gravelly materials. For tests on crushed limestone the increase of $G_{\max}$ with increasing d_{50} could be partly explained by the accompanying decrease of C_u. However, this is not the case for a comparison of two river gravels with Ottawa sand. Although C_u was significantly larger for the river gravels, their $G_{\max}$-values were larger than those measured for Ottawa sand. Tests on gravel-sand-silt mixtures showed that although these materials contained large fractions of gravel-sized particles, the $G_{\max}$-values measured were smaller than for the uniform sands. This may be due to the fines content as demonstrated also by the tests of Iwasaki & Tatsuoka [23] (Fig. 1b).

Although not studied in the present paper, major findings concerning the influence of the grain size distribution curve on the accumulation of residual strain (or excess pore water pressure in the undrained case) due to a cyclic loading with larger amplitudes are briefly summarized in the following. Lee & Fitton [29] performed undrained cyclic tests on sands with different values of d_{50}. They found a minimum cyclic undrained strength at $d_{50} = 0.1$ mm. In accordance with the data of Lee & Fitton [29] for $d_{50} > 0.1$ mm, Castro & Poulos [8] observed a faster increase of the excess pore water pressure in materials with a lower value of d_{10}. Vaid et al. [50] and also Kokusho et al. [26] compared the liquefaction resistance of sands with different C_u-values. For a constant relative density D_r, they could not find a significant influence of C_u. A similar conclusion was drawn by Duku et al. [12] regarding the accumulation of strain under drained conditions. From undrained cyclic tests it is well known that non-plastic fines decrease the liquefaction resistance while cohesive fines increase it (Towhata [49]). Furthermore, several researchers reported on a higher liquefaction resistance for gravelly materials in comparison to sand (Ishihara [22]).

Tested material

The present study was performed with a natural quartz sand obtained from a sand pit near Dorsten, Germany. The grain shape is sub-angular. For the finer fractions the grain shape was examined using a microscope. Based on the comparison of scaled photographs the grain shape of the different fractions was found to be quite similar. The sand was sieved into 25 gradations with grain sizes between 0.063 and 16 mm. These gradations were mixed to produce the grain size distribution curves depicted in Fig. 2. The curves are linear in the semi-logarithmic scale (that is because the sands are denoted "Lx"). The influence of the mean grain size d_{50} was studied in tests on the sands and gravels L1 to L8 (Fig. 2a). The gravel L9 is too coarse to be tested in the RC device (sample diameter $d = 10$ cm). L1 to L8 have a identical coefficient of uniformity of $C_u = 1.5$ and different mean grain sizes in the range $0.1 \leq d_{50} \leq 6$ mm. Three test series with different mean grain sizes have been performed on the influence of C_u (Fig. 2b). The mean grain size was $d_{50} = 0.2$ mm for sands L2, L24 to L26, $d_{50} = 0.6$ mm for sands L4, L10 to L16, and $d_{50} = 2$ mm for sands L6, L17 to L23. The coefficient of uniformity varied in the range $1.5 \leq C_u \leq 8$. The d_{50}- and C_u-values of the 25 tested grain size distribution curves are summarized in Table 1.

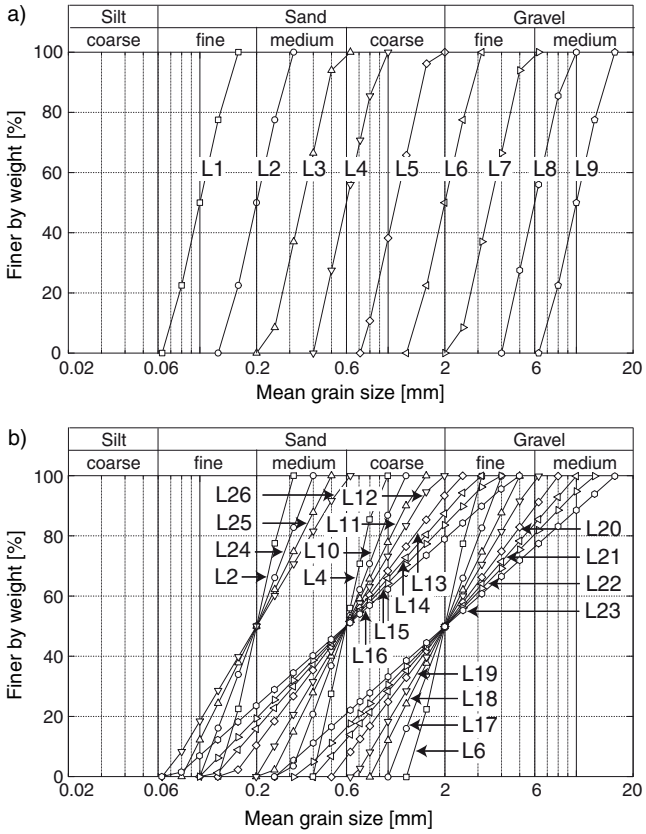

Fig. 2: Tested grain size distribution curves

Test device, specimen preparation and testing procedure

The resonant column (RC) device used for the present study is shown in Fig. 3. It is of the "free - free" type, meaning both the top and the base mass are freely rotatable. The cuboidal top mass is equipped with two electrodynamic exciters which each accelerate a small mass. This acceleration and the resulting acceleration of the top mass are measured with acceleration transducers. From these signals the applied torsional moment $M(t)$ and the twisting angle $\phi(t)$ about the vertical axis of the specimen can be calculated. The system is enclosed in a pressure cell which can sustain cell pressures σ_3 up to 800 kPa. The state of stress is almost isotropic. A small stress anisotropy results from the weight of the top mass ($m \approx 9$ kg), such that the vertical stress σ_1 is slightly higher than the lateral one σ_3. However, for higher cell pressures this anisotropy is of secondary importance. Furthermore, test results of Yu & Richart [56] reveal that a stress anisotropy becomes significant only near the failure stress.

A sinusoidal electrical signal is generated by a function generator, amplified and applied to the electrodynamic exciters. The frequency of excitation is varied until the resonant frequency f_R of the system composed of the two end

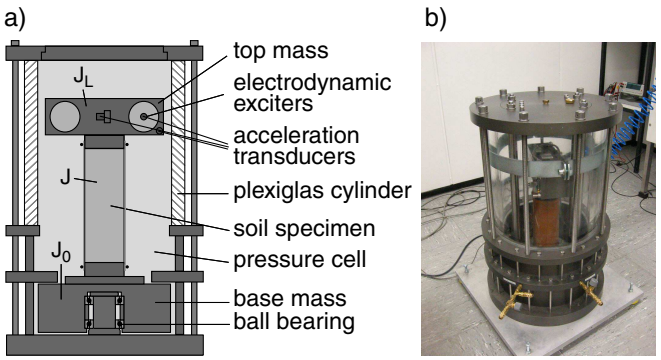

Fig. 3: Resonant Column device used for the present study: a) scheme and b) photo

masses and the specimen has been found. By definition, this is the case when $M(t)$ and $\phi(t)$ have a phase-shift of $\pi/2$ in time t (i.e. if the axes of the *Lissajous* figure are parallel to the ϕ- and M-axes). The secant shear modulus

$$G_{\text{sec}} = \left(\frac{2\pi\ h\ f_R}{a}\right)^2 \varrho \tag{4}$$

is calculated from the resonant frequency, the height h and the density ϱ of the specimen. The parameter a is obtained from Eq. (5):

$$a\ \tan(a) - \frac{J^2}{J_0\ J_L}\ \frac{\tan(a)}{a} = \frac{J}{J_0} + \frac{J}{J_L} \tag{5}$$

In Eq. (5) J, $J_0 = 1.176$ kg m^2 and $J_L = 0.0663$ kg m^2 are the polar mass moments of inertia of the specimen, the base mass and the top mass, respectively (Fig. 3a). Different shear strain amplitudes can be tested by varying the amplitude of the torsional excitation.

All tested specimens had a full cross section and measured $d = 10$ cm in diameter and $h = 20$ cm in height. They were tested under air-dry conditions. The specimens were prepared using the pluviation technique. Different initial densities were achieved by varying the size of the outlet of the funnel while keeping the drop height constant.

The nearly isotropic stress was increased in seven steps from $p = 50$ kPa over $p = 75$, 100, 150, 200 and 300 kPa to $p = 400$ kPa. The compaction of the soil was determined by means of non-contact displacement transducers. At each pressure p the small strain shear modulus $G_{\max}$ was measured after a short resting period of 5 minutes. At $p = 400$ kPa the curves $G_{\text{sec}}(\gamma)$ and $D(\gamma)$ (damping ratio) were measured. For each sand several such tests with different initial relative densities $D_{r0} = (\varrho_{d0} - \varrho_{d,\min})/(\varrho_{d,\max} - \varrho_{d,\min})$ were performed, with $\varrho_{d,\min}$ and $\varrho_{d,\max}$ being the minimum and maximum dry densities, respectively (see Table 1, determined according to DIN 18126 [1]).

Test results

The measured shear moduli $G_{\max}$ for most of the 25 grain size distribution curves are given as a function of void ratio e and for different mean pressures p in Fig. 4. For all tested sands the well-known decrease of $G_{\max}$ with increasing void ratio e was observed. Fig. 5 shows exemplary curves of $G_{\max}$ versus mean pressure p which are nearly linear in the double-logarithmic scale and can be described by $G_{\max} \sim p^n$.

Fig. 6 compares the $G_{\max}$-values for the eight materials L1 to L8 with the same $C_u = 1.5$ but with different mean grain sizes $0.1 \le d_{50} \le 6$ mm. Independent of the pressure p, the data points for the seven sands L1 to L7 lay on a unique curve, demonstrating that for a constant void ratio the variation in d_{50} does not influence $G_{\max}$. The values of the gravel L8 lay slightly below those of L1 to L7. Martinez [33] demonstrated that these lower values are due to an insufficient interlocking between the tested material and the end plates which were glued with coarse sand. In a test performed with end plates equipped with small wings penetrating into the specimen, the $G_{\max}$-values of L8 coincided with those of the sands L1 to L7. Thus, from this test series it may be concluded that for a constant void ratio d_{50} does not influence $G_{\max}$, at least in the range of the tested d_{50}-values. Thus, the mean grain size need not be considered in an empirical equation for $G_{\max}$. Fig. 6 confirms the test results of Iwasaki & Tatsuoka [23]. The d_{50}-independence of $G_{\max}$ is also reasonable from the micromechanical point of view as explained later. However, higher $G_{\max}$-values reported for materials with a high content of large gravel particles (see Hardin & Kalinski [18]) cannot be excluded. Such coarse materials could not have been tested in the available RC device due to the relatively small specimen size ($d = 10$ cm). The slight increase of $G_{\max}$ with increasing d_{50} sporadically reported also for pure sands (e.g. Menq & Stokoe [34]) is not confirmed by the results of the present study. Possibly, it could be due to variations in the grain shape.

In Fig. 7 the data of the test series on the influence of C_u are combined. The data of the two or three sands (e.g. L24, L10 and L17) with equal C_u but different d_{50} fall together confirming the d_{50}-independence of $G_{\max}$ also for $C_u > 1.5$. For $e =$ constant the decrease of $G_{\max}$ with increasing C_u is obvious in Figs. 4 and 7. It becomes even more evident from the diagram in Fig. 8 where the $G_{\max}$-values at $e = 0.55$ are plotted versus C_u. For $p = 50$ kPa the shear modulus (mean value of the three test series) is $G_{\max} = 115$ MPa for the sand with $C_u = 1.5$, but for the sand with $C_u = 8$ it is only $G_{\max} = 53$ MPa (corresponding to a 54 % decrease). For $p = 400$ kPa the values are $G_{\max} = 277$ MPa for $C_u = 1.5$, and $G_{\max} = 169$ MPa for $C_u = 8$ (39 % decrease). The ratio of the shear modulus $G_{\max}(C_u)$ and the respective value $G_{\max}(C_u = 1.5)$ for the uniform sands has been calculated. The range of this ratio has been added to Fig. 1b. The magnitude of the decrease of $G_{\max}$ measured in the present study is similar to that observed by Iwasaki & Tatsuoka [23]. However, the shape of the curves is somewhat different. It has to be considered that for most of the tested sands, Iwasaki & Tatsuoka [23] performed only one test with a high relative density. Thus, the available data is limited. Furthermore, the data points obtained by Iwasaki & Tatsuoka [23] and shown in Fig. 1b correspond to different grain shapes.

In Fig. 7 the curves predicted by Hardin's equation (2) with the constants for round and for angular grains have been supplemented. In general, in the RC tests presented in this paper the void ratio-dependence was found to be slightly larger than predicted by Eq. (2). From Fig. 7 it is obvious that Eq. (2) overestimates the $G_{\max}$-values for well-graded soils, especially at large void ratios, i.e small

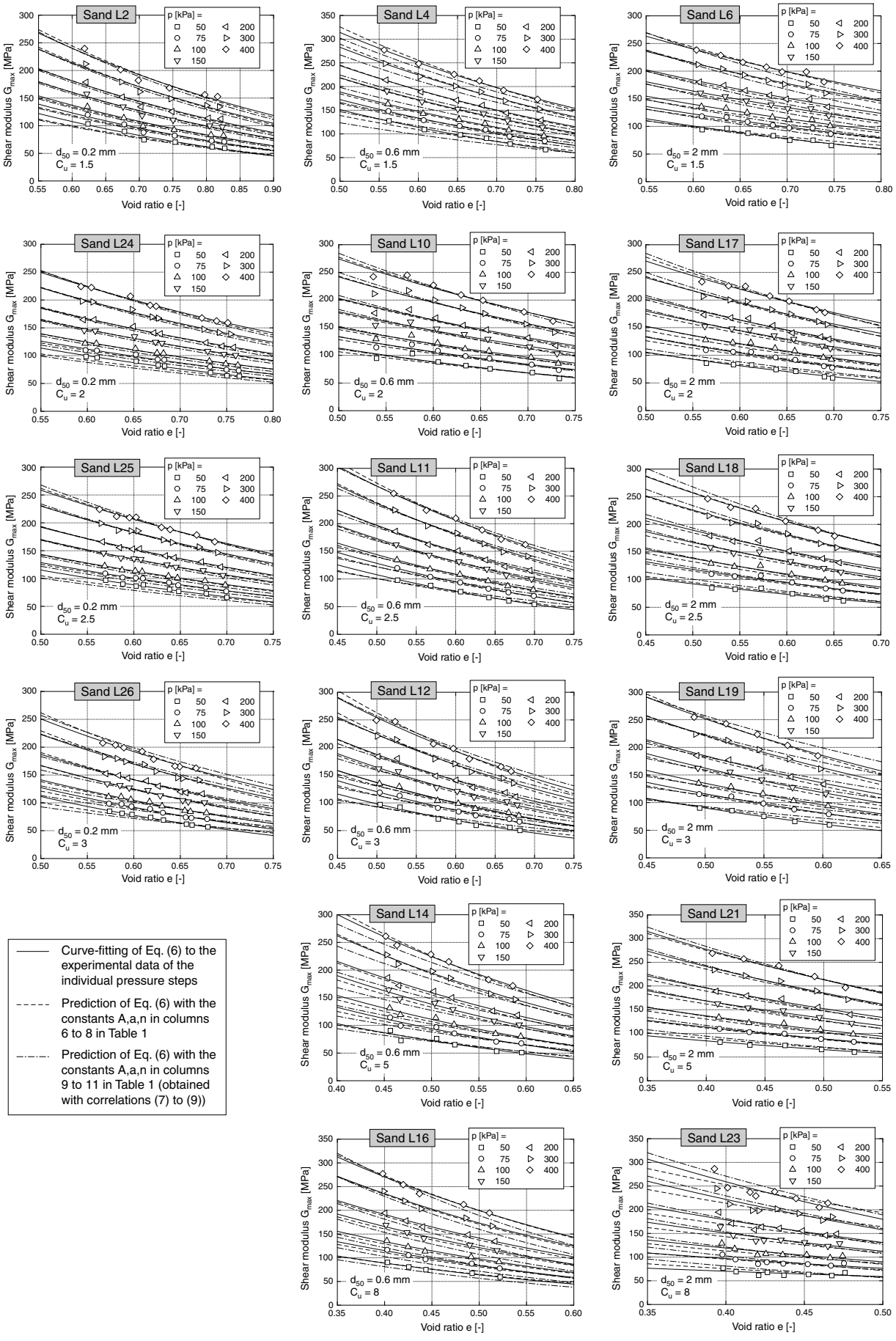

Fig. 4: *Comparison of measured and predicted shear moduli* $G_{\max}(e,p)$

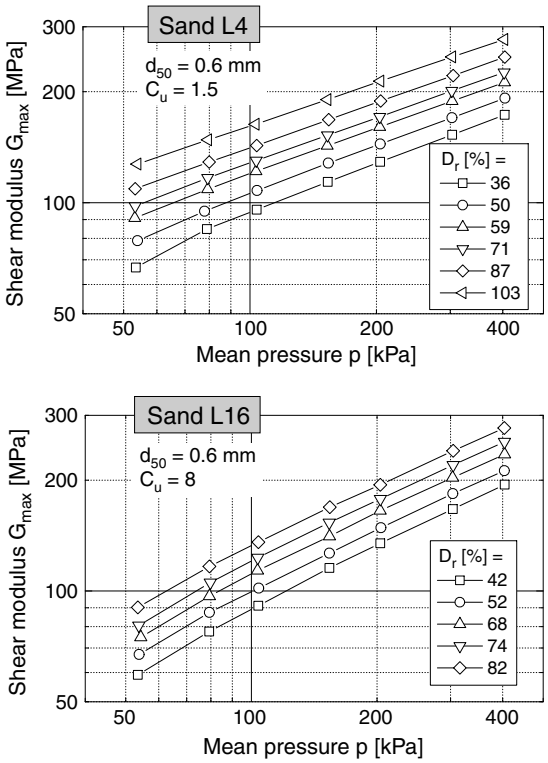

Fig. 5: Increase of shear modulus $G_{\max}$ with pressure p for sands L4 and L16

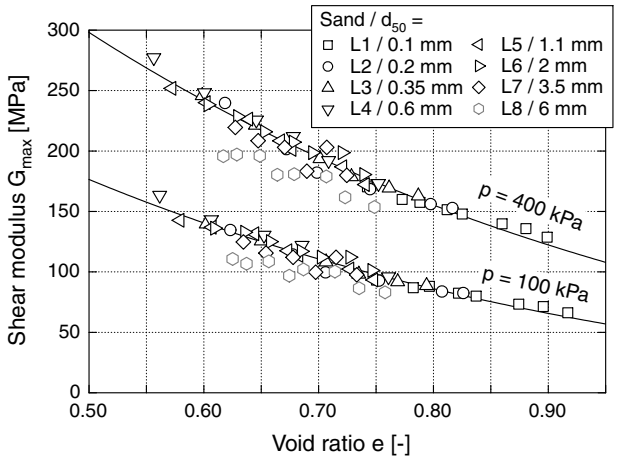

Fig. 6: Comparison of $G_{\max}(e)$ of the eight sands L1 - L8 (C_u = 1.5, 0.1 $\leq d_{50} \leq$ 6 mm) for pressures p = 100 kPa and p = 400 kPa

relative densities. Furthermore, Eq. (2) may underestimate the shear moduli for poorly graded soils at small void ratios.

The modulus coefficient $K_{2,\max}$ used in Eq. (3) was also calculated for each sand. For some of the sands it is shown in Fig. 9 as a function of void ratio. The decrease of $K_{2,\max}$ with increasing void ratio is apparent in Fig. 9. The exponent n describing the pressure-dependence $G_{\max} \sim p^n$ obtained for the 25 different sands lie in the range between 0.41 and 0.58 (Table 1, column 8). Thus, the exponent 0.5 in Eq. (3) is an appropriate average value. The $K_{2,\max}$-values obtained for the 25 grain size distribution curves lie between 30 for loose sands and 80 for dense sands (Figure 9). This range is in good accordance with the values

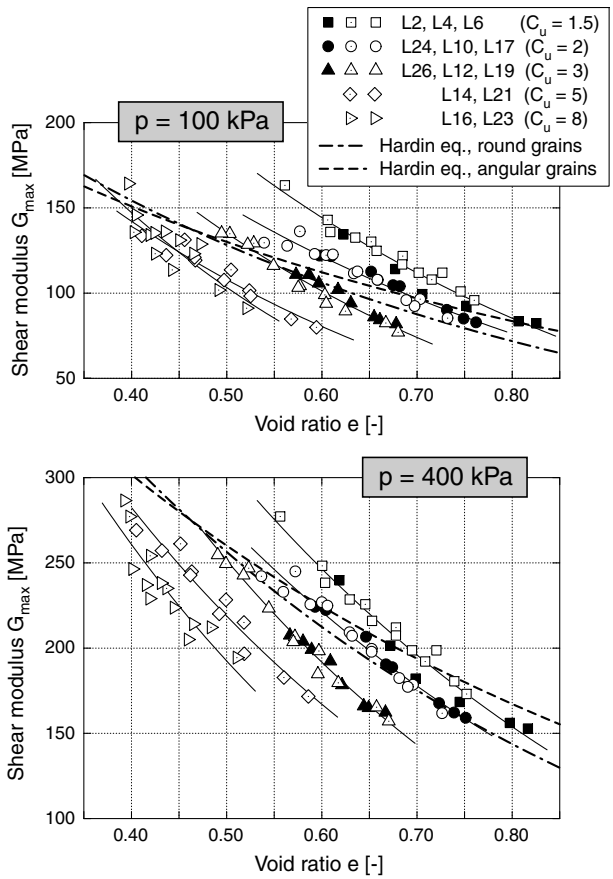

Fig. 7: Comparison of $G_{\max}(e)$ of the grain size distribution curves with different C_u-values. Continuous lines are best-fit curves of the combined data obtained for the two or three sands having the same C_u-value.

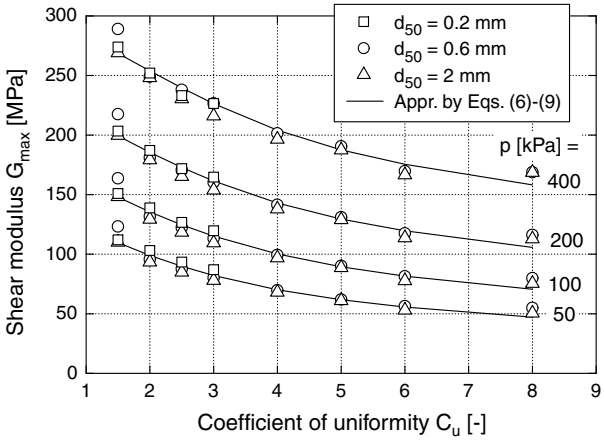

Fig. 8: Shear modulus $G_{\max}$ at $e = 0.55$ as a function of C_u for different pressures p

reported by Seed et al. [45] for laboratory tests on reconstituted sand samples ($30 \leq K_{2,\max} \leq 75$).

In order to investigate if the small strain shear modulus of the 25 tested grain size distribution curves can be described by a unique function of relative density, $G_{\max}$ was plotted versus D_r in Fig. 10. Fig. 10 reveals that the scatter of data is quite significant, especially for the higher pressures. The $G_{\max}$-values of the sands with a mean grain size $d_{50} = 0.2$ mm are located at the lower boundary of the clouds of data points while the $G_{\max}$-values of the sands with $d_{50} = 2$ mm tend to lay at the upper boundary. That means that for D_r = constant, $G_{\max}$ slightly increases with increasing d_{50}. No clear tendency concerning the influence of C_u could be found from the data in Fig. 10. This conclusion is not far from that of Menq & Stokoe [34] who found only a slight increase of $G_{\max}$ with increasing C_u for D_r = constant.

Therefore, while considering a constant void ratio there is a large influence of the coefficient of uniformity on the small strain shear modulus, this influence is rather small when a constant relative density D_r is taken as the basis of comparison. This finding can be explained by the fact, that simultaneously with $G_{\max}$ the maximum and minimum void ratios of a sand decrease with increasing value of C_u. This becomes clear from the $e_{\min}$- and $e_{\max}$-data given in columns 4 and 5 of Table 1. A decrease of the minimum and maximum void ratios with increasing C_u has been also reported by Kokusho et al. [26]. An increase of the fines content FC below a so-called "limiting fines content" has a similar effect on $e_{\min}$ and $e_{\max}$ (Lade et al. [28], Polito & Martin [37]). Therefore, considering a constant void ratio, larger values of C_u mean lower relative densities D_r. Vice versa, considering a constant relative density, larger values of C_u implicate lower void ratios e. Thus, for D_r = constant the decrease of $G_{\max}$ with increasing C_u may be somewhat compensated by the increase of $G_{\max}$ due to the decrease of the void ratio.

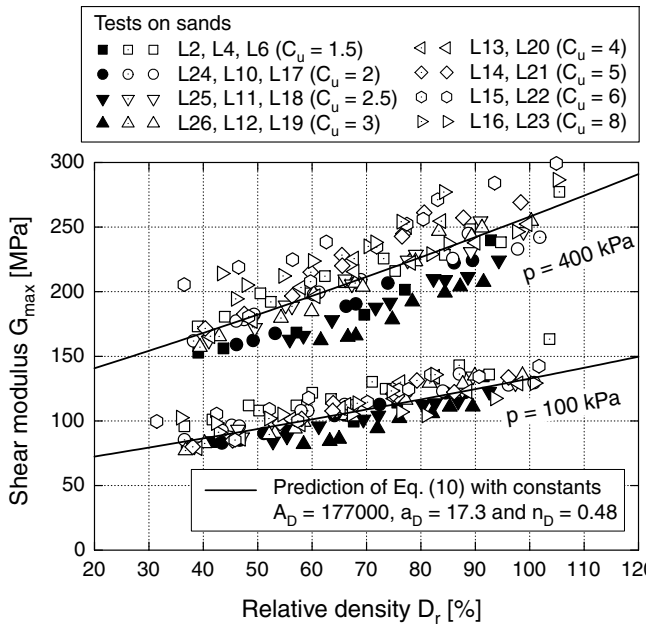

Fig. 10: Small strain shear modulus $G_{\max}$ as a function of relative density D_r

A similar diagram is given for the modulus coefficient $K_{2,\max}$ in Fig. 11. The presented data corresponds to pressures $p = 100$ kPa and $p = 400$ kPa. Similar to the data of $G_{\max}$ in Fig. 10, the data of $K_{2,\max}$ versus D_r in Fig. 11 shows a quite large scatter. Fig. 11 also confirms the range of $K_{2,\max}$-values reported by Seed et al. [45].

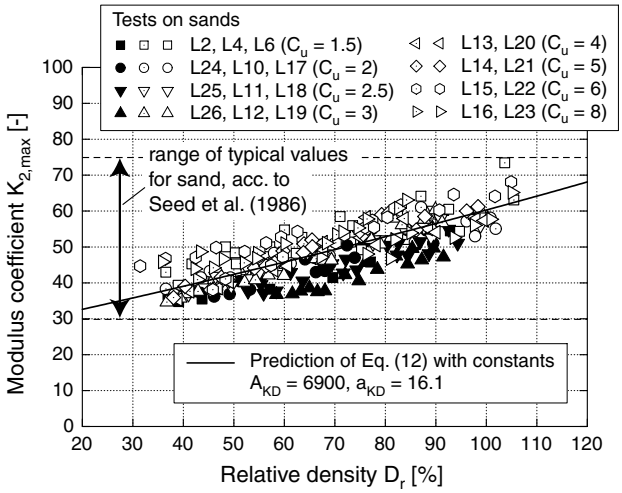

Fig. 11: Modulus coefficient $K_{2,\max}$ as a function of relative density D_r, data for $p = 100$ kPa and $p = 400$ kPa

Correlations for $G_{\max}$ and $K_{2,\max}$

A discussion on four different types of correlations for $G_{\max}$ and $K_{2,\max}$ follows. The relationships are based either on Hardin's equation (2) or on the formula (3) proposed by Seed & Idriss [44]. The formulas may be applied either with the void ratio e or with the relative density D_r as input variables.

1. Hardin's equation (2) in its dimensionless form

$$G_{\max} = A \underbrace{\frac{(a-e)^2}{1+e}}_{F(e)} \underbrace{{p_{\text{atm}}}^{1-n}\, p^n}_{F(p)} \tag{6}$$

with atmospheric pressure $p_{\text{atm}} = 100$ kPa, has been fitted separately to the test data for each grain size distribution curve. First, the constant a was determined for a certain pressure p by fitting the function $f(e) = k\ F(e)$ to the data $G_{\max}(e)$ (the constant k is not used further). The a-value in column 7 of Table 1 is the mean value of the seven values obtained for the different pressures p. Afterwards the shear moduli were divided by the void ratio function $F(e)$ and the data $G_{\max}/F(e)$ was plotted versus p. The function $f(p) = k\ F(p)$ was fitted to the data of each test resulting in the exponent n. The n-value in column 8 of Table 1 is the mean value for the different tests. The data $G_{\max}/F(e)/F(p)$ is equal to the constant A. First, a mean value of A was determined for each test. Afterwards the values from the different tests were averaged resulting in the A-values given in column 6 of Table 1.

The good approximation of Eq. (6) with the constants A, a and n given in columns 6 to 8 of Table 1 is demonstrated in Fig. 4 where the prediction is shown as the

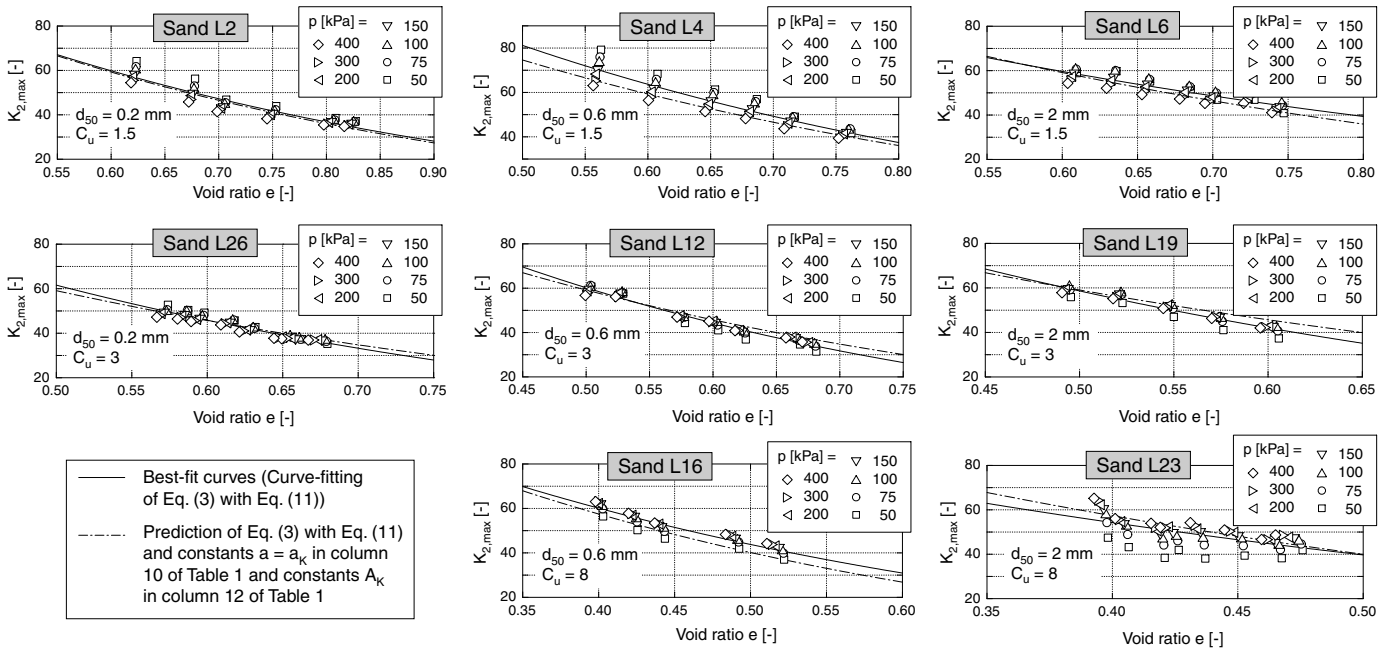

Fig. 9: *Curves $K_{2,\max}(e)$ for some of the tested grain size distribution curves*

dashed curves. In most cases the deviation from the best-fit curve (solid line, resulting from the fitting of $f = k\ F(e)$ to the data of each pressure step) is small. Eq. (6), with the constants A, a and n given in columns 6 to 8 of Table 1, has also been used to generate the data points in Fig. 8.

The aim of the current study was to develop a unique formula for the prediction of $G_{\max}$ for different grain size distribution curves. For this purpose correlations of the parameters A, a and n in Eq. (6) with the coefficient of uniformity were developed. In Fig. 12a the parameter a is plotted versus C_u. For each sand the seven values for the seven tested pressures are given. The decrease of a with increasing C_u may be described by the exponential function

$$a \quad = \quad c_1\ \exp(-c_2\ C_u) \tag{7}$$

with constants $c_1 = 1.94$ and $c_2 = 0.066$ (solid line in Fig. 12a). Fig. 12b shows the parameter n as a function of C_u. The exponent n increases with increasing C_u which has been also reported by Menq & Stokoe [34]. It can be expressed by the potential function

$$n \quad = \quad c_3\ {C_u}^{c_4} \tag{8}$$

with constants $c_3 = 0.40$ and $c_4 = 0.18$. The parameters a and n were calculated from Eqs. (7) and (8) for each tested grain size distribution curve and are summarized in columns 10 and 11 of Table 1. Using these values the functions $F(e)$ and $F(p)$ were re-calculated and from the data $G_{\max}/F(e)/F(p)$ the parameter A was determined. In Fig. 12c it is plotted versus C_u. The relationship $A(C_u)$ may be approximated by a function consisting of a constant and a potential portion:

$$A \quad = \quad c_5 + c_6\ {C_u}^{c_7} \tag{9}$$

with constants $c_5 = 1563$, $c_6 = 3.13$ and $c_7 = 2.98$. In contrast to $G_{\max}$ the parameter A increases with increasing C_u. This is due to the functions $a(C_u)$ and $n(C_u)$ which for $A =$ constant would predict a stronger decrease of $G_{\max}$ with C_u as experimentally observed. The function $A(C_u)$ has to compensate this. It should be mentioned that small variations in a and n cause large deviations in A. The A-values calculated from Eq. (9) for the tested grain size distribution curves are collected in column 9 of Table 1.

The $G_{\max}$-values predicted by Eq. (6) with the parameters A, a and n obtained from Eqs. (7), (8) and (9) are compared to the test data in Fig. 4 (dot-dashed lines). An alternative presentation is given in the first row of diagrams in Fig. 13 where the predicted $G_{\max}$-values (for the same e and p) are plotted versus the measured ones. Since the deviations of the data from the line $G_{\max}^{\text{pred.}} = G_{\max}^{\text{meas.}}$ are small, the good prediction of the proposed correlations is confirmed. Another proof for the proposed correlations are the predicted $G_{\max}$-values for $e = 0.55$ in Fig. 8 (solid lines). Eqs. (6) to (9) describe well the decrease of $G_{\max}$ with C_u.

In the following a comparison of the $G_{\max}$-values predicted by Hardin's equation (2) with its commonly used constants and by Eqs. (6) to (9) is undertaken for a void ratio $e = 0.55$. For a well-graded sand ($C_u = 8$) and a small pressure $p = 50$ kPa, Hardin's equation predicts a shear stiffness of 1.75 (round grains) or 1.81 (angular grains) times larger than obtained from Eqs. (6) to (9). For the highest tested pressure $p = 400$ kPa the factors are 1.48 or 1.53, respectively. For a poorly-graded sand ($C_u = 1.5$) and $p = 50$ kPa, Hardin's equation delivers 0.75 (round grains) or 0.87 (angular grains) times smaller values than Eqs. (6) to (9). The deviation for $p = 400$ kPa is slightly less (factors 0.78 and 0.90, respectively). Thus, especially for well-graded soils there is a quite large difference

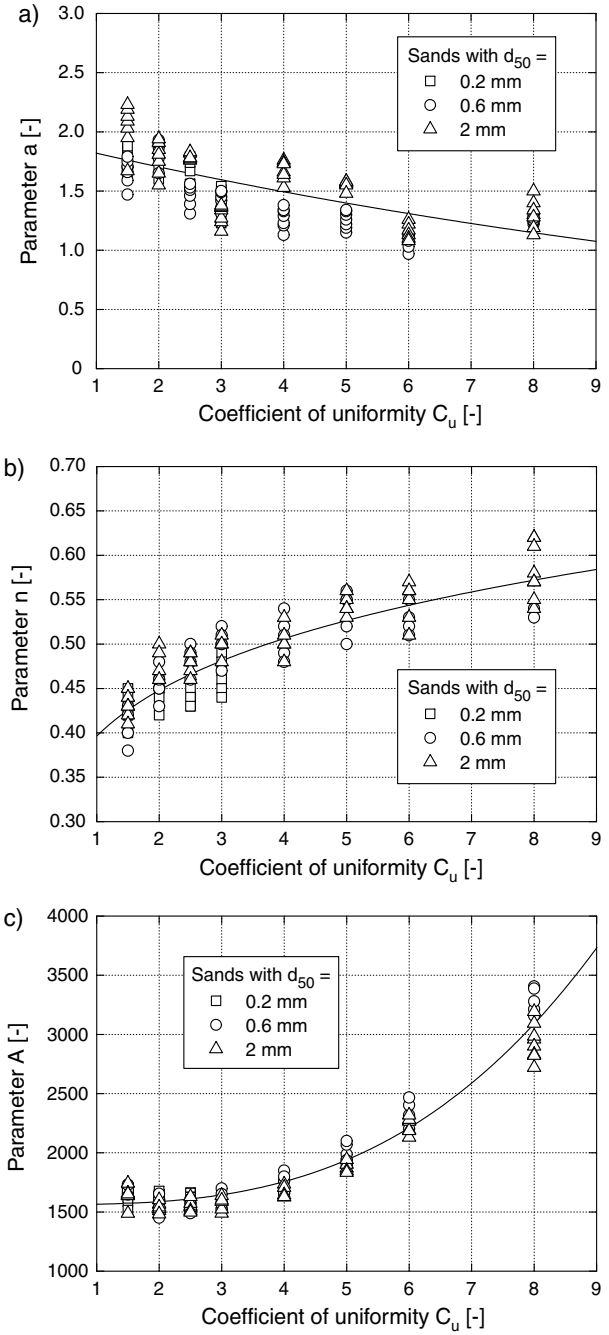

Fig. 12: Parameters a, n and A in dependence of C_u

between the predictions of Hardin's equation with its commonly used constants and of the predictions using the correlations developed in the present study.

2. Next, a correlation of $G_{\max}$ with relative density D_r was developed. The function

$$G_{\max} = A_D \underbrace{\frac{1+D_r/100}{(a_D - D_r/100)^2}}_{F(D_r)} {p_{\mathrm{atm}}}^{1-n_D} p^{n_D} \quad (10)$$

was fitted to the data in Fig. 10 (solid curves) resulting in constants $A_D = 177000$, $a_D = 17.3$ and $n_D = 0.48$. As apparent from Fig. 10 and also from the second row of diagrams in Fig. 13 the prediction of $G_{\max}$ by Eq. (10) is less accurate than the prediction by Eqs. (6) to (9).

3. Using Eq. (3) the dependence of the modulus coefficient $K_{2,\max}$ on void ratio e may be described by

$$K_{2,\max} = A_K \frac{(a_K - e)^2}{1+e} \quad (11)$$

with parameters A_K and a_K. Eq. (11) was fitted to the test data given in Fig. 9 (solid curves). Since the sands with low C_u-values have exponents $n < 0.5$ (Table 1, column 8), the best-fit curve underestimates $K_{2,\max}$ for low pressures and overestimates it for high pressures. For the sands with high C_u-values it is the other way around. For intermediate C_u-values there is nearly no pressure-dependence of $K_{2,\max}$ due to $n \approx 0.5$. The parameters A_K and a_K in Eq. (11) can be formulated as functions of C_u. The dependence $a_K(C_u)$ is the same as shown in Fig. 12a. Thus, for a_K in Eq. (11), again Eq. (7) with constants $c_1 = 1.94$ and $c_2 = 0.066$ is applicable. Analyzing the test data with these a_K-values, the constant A_k is plotted versus C_u in Fig. 14. The increase of A_k with increasing C_u-value can be approximated by Eq. (9) with constants $c_5 = 69.9$, $c_6 = 0.21$ and $c_7 = 2.84$ (see A_K-values in Table 1, column 12). The quite good prediction of Eq. (11) with the proposed correlations $A_K(C_u)$ and $a_K(C_u)$ can be seen in Fig. 9 (dot-dashed curves) and in the third row of diagrams in Fig. 13. However, due to the fixed pressure-dependence ($n = 0.5$) the predicted $G_{\max}$-values are less accurate than those obtained from Eqs. (6) to (9).

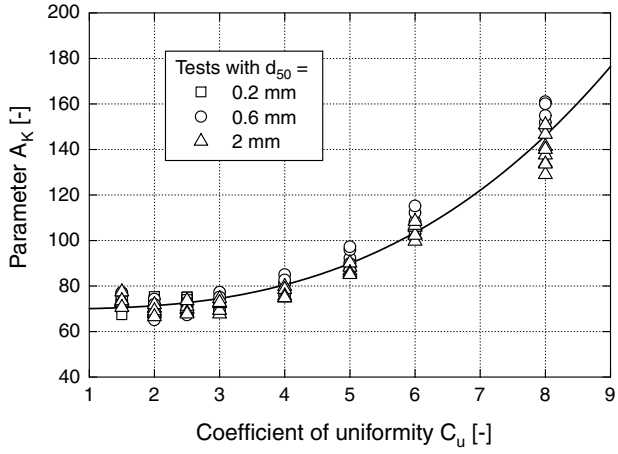

Fig. 14: Parameter A_k of Eq. (11) as a function of C_u

4. The last empirical formula correlates $K_{2,\max}$ with relative density D_r. The function

$$K_{2,\max} = A_{KD} \frac{1+D_r/100}{(a_{KD} - D_r/100)^2} \quad (12)$$

with the constants $A_{KD} = 6900$ and $a_{KD} = 16.1$ could be fitted to the data in Fig. 11 (solid curve). The $G_{\max}$-values predicted by Eq. (12) are plotted versus the measured ones in the last row of diagrams in Fig. 13.

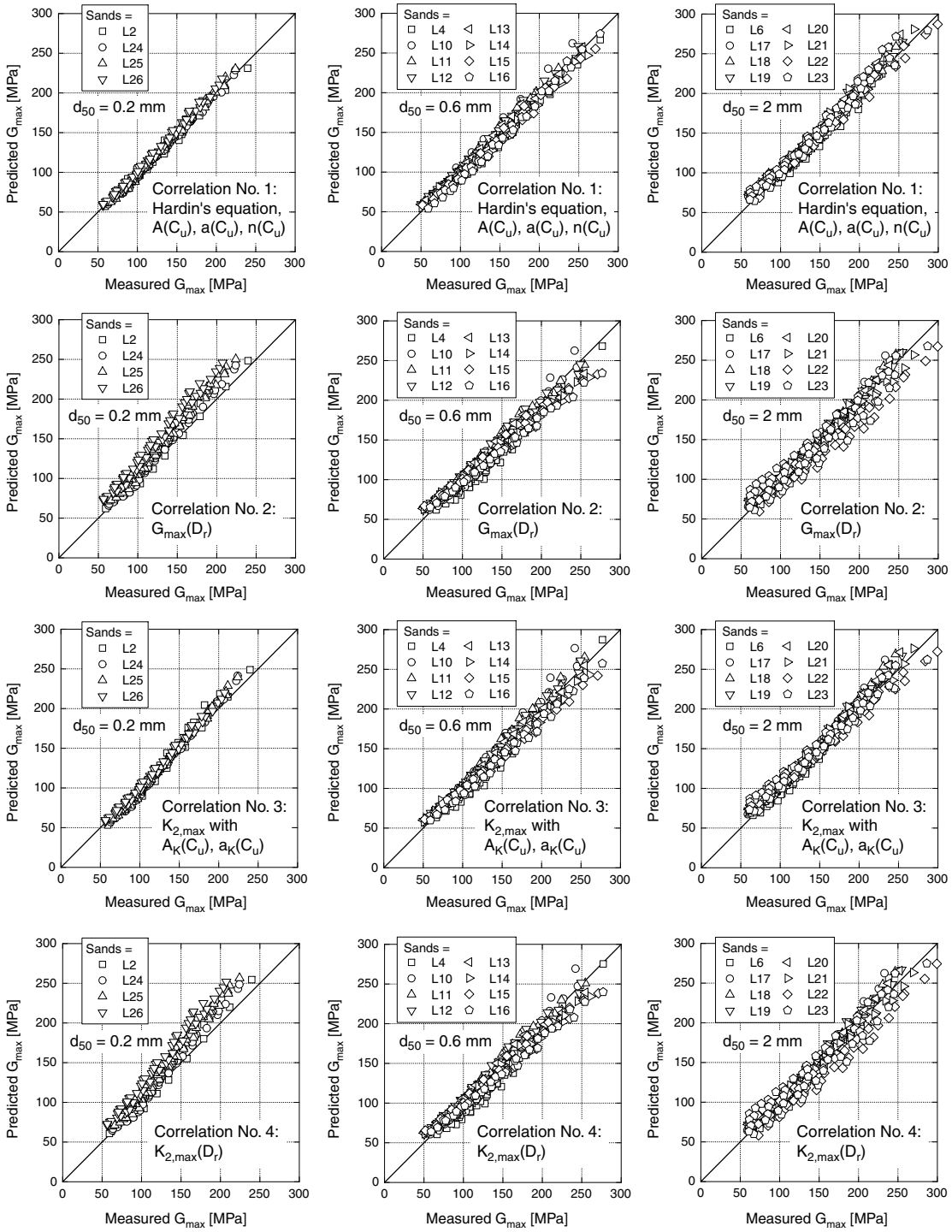

Fig. 13: *Shear moduli predicted by the four proposed correlations versus measured $G_{\max}$-values*

The quality of prediction is similar to that of Eq. (10) correlating $G_{\max}$ with D_r.

The empirical formulas for $G_{\max}$ and $K_{2,\max}$ which are formulated in terms of void ratio and which use correlations of the parameters A, a and n with C_u, are generally more precise than the equations which establish correlations of $G_{\max}$ and $K_{2,\max}$ with relative density D_r. Thus, whenever information on void ratio is available, the application of Eqs. (6) to (9) is recommended. If a formulation with the modulus coefficient $K_{2,\max}$ is preferred, one should use Eq. (11) with the corresponding correlations $A_k(C_u)$ and $a_k(C_u)$. For rough estimations the empirical equations formulated in terms of relative density may be sufficient.

Comparison of the predictions of the proposed correlations with $G_{\max}$-data from the literature

A comparison of $G_{\max}$-values predicted by the correlations presented in the previous section with $G_{\max}$-data from the literature has been undertaken. Fig. 15 collects approx. 650 values of $G_{\max}$ measured in the laboratory by different researchers on different types of sands at different stress levels

1	2	3	4	5	6	7	8	9	10	11	12
Sand	d_{50} [mm]	C_u [-]	$\varrho_{d,\min}$ [g/cm^3]	$\varrho_{d,\max}$ [g/cm^3]	From fitting of (6) for each sand			From correlations (7) to (9)			$K_{2,\max}$ Eq. (3)
					A	a	n	A	a	n	A_K
L1	0.1	1.5	1.246	1.622	636	2.34	0.44	1573	1.76	0.43	70.6
L2	0.2	1.5	1.329	1.661	1521	1.79	0.43	1573	1.76	0.43	70.6
L3	0.35	1.5	1.372	1.666	1620	1.77	0.42	1573	1.76	0.43	70.6
L4	0.6	1.5	1.401	1.687	2023	1.67	0.41	1573	1.76	0.43	70.6
L5	1.1	1.5	1.410	1.678	1570	1.77	0.43	1573	1.76	0.43	70.6
L6	2	1.5	1.412	1.666	1035	2.04	0.43	1573	1.76	0.43	70.6
L7	3.5	1.5	1.458	1.630	852	2.13	0.45	1573	1.76	0.43	70.6
L8	6	1.5	1.473	1.622	734	2.16	0.45	1573	1.76	0.43	70.6
L10	0.6	2	1.421	1.719	1207	1.85	0.46	1588	1.70	0.45	71.4
L11	0.6	2.5	1.428	1.773	2240	1.47	0.48	1611	1.64	0.47	72.7
L12	0.6	3	1.449	1.798	2489	1.39	0.50	1646	1.59	0.49	74.7
L13	0.6	4	1.479	1.874	2969	1.27	0.51	1758	1.49	0.51	80.7
L14	0.6	5	1.516	1.900	2771	1.26	0.54	1942	1.39	0.53	90.2
L15	0.6	6	1.542	1.910	4489	1.08	0.53	2215	1.31	0.55	104.0
L16	0.6	8	1.584	1.954	2388	1.27	0.54	3100	1.14	0.58	147.0
L17	2	2	1.451	1.705	1325	1.78	0.47	1588	1.70	0.45	71.4
L18	2	2.5	1.464	1.752	1194	1.79	0.48	1611	1.64	0.47	72.7
L19	2	3	1.486	1.777	3018	1.30	0.49	1646	1.59	0.49	74.7
L20	2	4	1.534	1.841	1197	1.67	0.51	1758	1.49	0.51	80.7
L21	2	5	1.556	1.891	1402	1.54	0.54	1942	1.39	0.53	90.2
L22	2	6	1.707	1.892	3345	1.15	0.55	2215	1.31	0.55	104.0
L23	2	8	1.743	1.895	1382	1.47	0.58	3100	1.14	0.58	147.0
L24	0.2	2	1.353	1.700	1446	1.77	0.43	1588	1.70	0.45	71.4
L25	0.2	2.5	1.368	1.715	1434	1.72	0.44	1611	1.64	0.47	72.7
L26	0.2	3	1.380	1.720	2451	1.42	0.46	1646	1.59	0.49	74.7

Table 1: Parameters d_{50}, C_u, $\varrho_{d,\min}$ and $\varrho_{d,\max}$ of the tested grain size distribution curves; Summary of the constants A, a and n used in the different correlations

and void ratios. The data were obtained either from RC tests, from measurements with bender elements or from hollow cylinder torsional shear tests. Only data for an isotropic first loading has been considered. An additional selection criterion was that information about the effective stress and about void ratio was available. Fig. 15 shows the $G_{\max}$-values predicted either by Eqs. (6) to (9) or by Eq. (10) as a function of the measured values. The predictions were calculated with the values of e, p, C_u, $\varrho_{d,\min}$ and $\varrho_{d,\max}$ given in the respective publications. Unfortunately, most of the "standard" sands (e.g. Ottawa Sand, Monterey No. 0 Sand, Toyoura Sand, Ticino Sand, Hostun Sand) which are frequently used for laboratory testing have a rather uniform grain size distribution curve. Measurements performed on well-graded sands are rare in the literature. In Fig. 15 it is distinguished between a round (upper row of diagrams), a subangular (middle row) and an angular grain shape (lower row).

The prediction of Eqs. (6) to (9) is shown on the left hand side of diagrams in Fig. 15. Considering a subangular grain shape (similar to the grain shape of the sand used for the present test series) most of the data points plot closely to the bisecting line. That means that the measured and the predicted $G_{\max}$-values coincide well. Although there is some scatter in the data for the angular grain shape, the tendency is also reproduced well by Eqs. (6) to (9). The $G_{\max}$-values given in the literature for sands with round grains are generally lower than those specified for a subangular or an angular grain shape (compare also Hardin & Richart [19] and the two sets of constants proposed for Eq. (2)). Accordingly, as apparent from Fig. 15 the new correlations over-estimate the $G_{\max}$-values for a round grain shape. Thus, in future Eqs. (6) to (9) should be extended by a reduction of $G_{\max}$ for sands with a round grain shape.

The prediction of Eq. (10) is given on the right hand side of diagrams in Fig. 15. For subangular grains once again most of the data points plot closely to the line described by $G_{\max}^{\text{pred.}} = G_{\max}^{\text{meas.}}$. The over-prediction of $G_{\max}$ for sands with round grains is considerably smaller when using Eq. (10) instead of Eqs. (6) to (9). However, Eq. (10) seems to over-predict the small strain shear modulus for an angular grain shape. This conclusion is based on limited test data, mainly on the results of Hardin & Richart [19] for a crushed sand, and will be inspected in future using the data from further RC tests.

Based on Fig. 15 it may be concluded that for sands with a subangular grain shape both correlations, Eqs. (6) to (9) and Eq. (10) deliver quite reasonable results. While for round grains the correlation of $G_{\max}$ with D_r as given in Eq. (10) works better, for angular grains Eqs. (6) to (9) deliver more realistic values. However, more data for sands with higher C_u-values and various grain shapes would be beneficial.

Application to in-situ soils

The present experimental study was performed with dry freshly pluviated specimens in the laboratory. The $G_{\max}$-values of in-situ soils may be larger, in particular due to

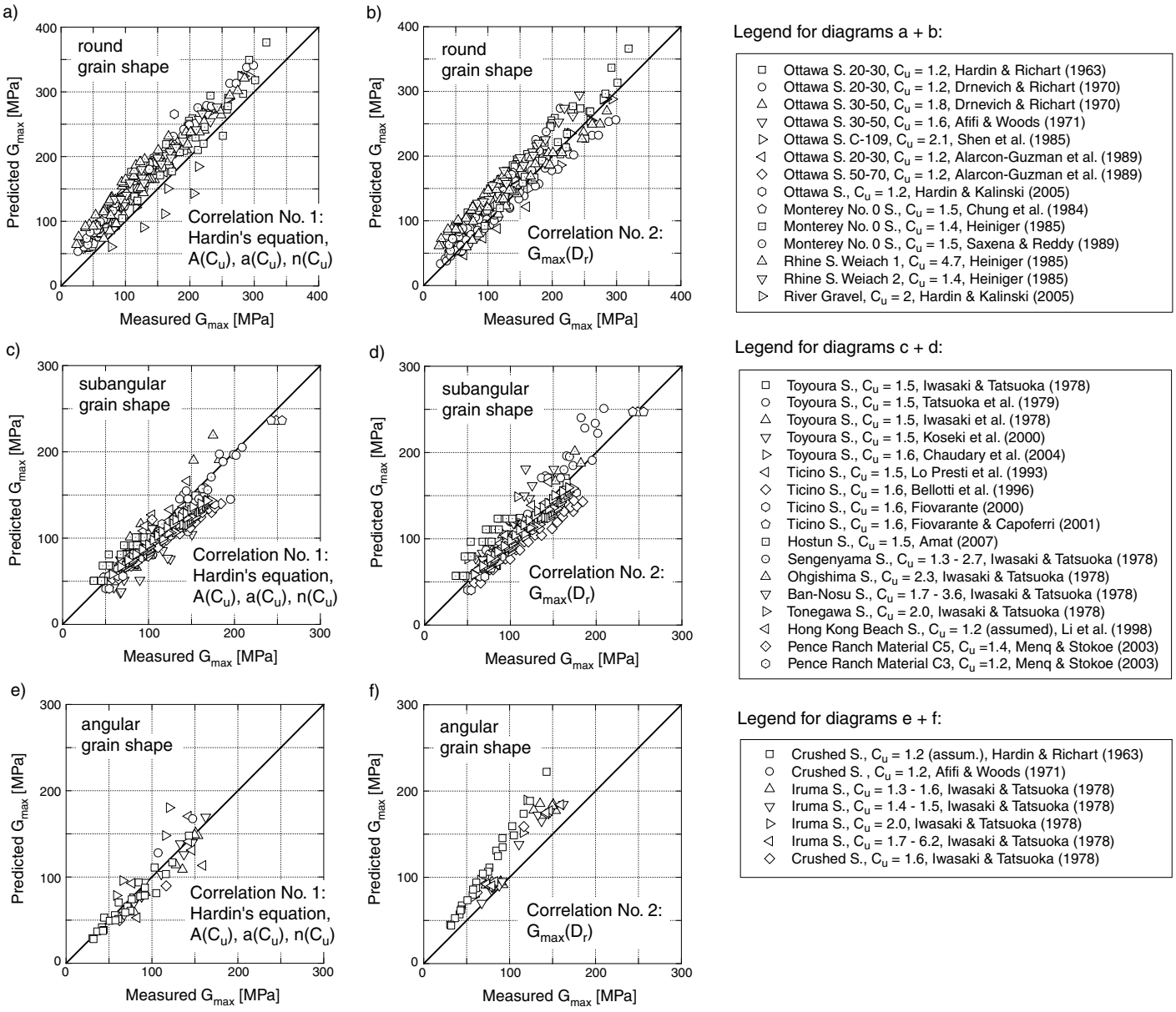

Fig. 15: *Comparison of the predictions by Eqs. (6) to (9) or by Eq. (10), respectively, with $G_{\max}$-data from the literature*

the effects of aging and moisture conditions.

Tatsuoka et al. [47] could not find a significant influence of the method of specimen preparation on the small-strain shear modulus of granular soils. Thus, independent of its initial fabric a young in-situ deposit of sand may have a similar $G_{\max}$-value as a freshly pluviated specimen in the laboratory.

Depending on the geological age of a sand deposit, aging effects may have significantly increased the small strain stiffness in comparison to a freshly pluviated sand sample tested in the laboratory. According to Afifi & Woods [3], Afifi & Richart [2] or Baxter [6], under constant stresses $G_{\max}$ increases approximately linear proportional to the logarithm of time. This increase can be described by

$$G_{\max}(t) \quad = \quad G_{\max}(t_0)\ [1 + N_G\ \ln(t/t_0)] \qquad (13)$$

with a reference time $t_0 \neq 0$ and an inclination factor N_G. The authors of the present paper have performed RC tests on a quartz sand similar to L4. During three weeks of sustained pressure a factor $N_G = 0.005$ was measured, almost independent of the initial density and of the confining pressure. N_G-values for different types of sands were also reported by Baxter [6]. If the geological age of a sand deposit is approximately known, the $G_{\max}(t_0)$-values from the laboratory tests could be corrected using Eq. (13) with t_0 = 5 min and $N_G = 0.005$.

While some researchers (e.g. Drnevich & Richart [11]) reported on a significant increase of $G_{\max}$ due to a cyclic preloading, more recent publications (e.g. Lo Presti et al. [31], Teachavorasinskun et al. [48], Li & Yang [30]) came to the conclusion that a cyclic preloading causes only minor changes of the small strain stiffness. The authors of the present paper have performed RC tests with various kinds of cyclic preloading on a quartz sand similar to L4 (Wichtmann & Triantafyllidis [54]). An influence of the cyclic preloading on small-strain stiffness could hardly be found. Thus, changes in the fabric of the soil skeleton due to a cyclic loading seem to have a rather small effect on

$G_{\max}$. This coincides with the conclusion of Tatsuoka et al. [47] regarding the insignificant influence of the initial fabric. A correction of the laboratory $G_{\max}$-data regarding a cyclic preloading seems not to be necessary.

For practical purposes the effect of the anisotropy of the effective stress in situ may be disregarded as well. Starting from the isotropic state, Yu & Richart [56] observed an almost linear decrease of $G_{\max}$ with increasing stress ratio σ_1/σ_3. However, the $G_{\max}$-values at $\sigma_1/\sigma_3 = 2$ were only approximately 5 % lower than the corresponding values at $\sigma_1/\sigma_3 = 1$.

In partly saturated soils, the capillary pressure p_c causes an increase of the effective stress and thus an increase of the small-strain shear stiffness compared to dry or fully saturated soils (Wu et al. [55], Qian et al. [38]). The effect can be considered by increasing the effective pressure p in the empirical equations for $G_{\max}$ by the capillary pressure p_c. Qian et al. [38] presented curves of $G_{\max}/G_{\max}^{\text{dry}}$ versus the degree of saturation S_r with $G_{\max}^{\text{dry}}$ being the small strain shear modulus of dry specimens. These curves were given for different types of sands, void ratios and confining stresses and may also be a useful tool for correcting the laboratory data to in-situ conditions.

Micromechanical explanation of the experimental observations

For small strain amplitudes, shear deformations are the result of particle distortion rather than sliding and rolling between particles (Gazetas [16]). The experimentally observed independence of the small-strain shear stiffness of the mean grain size d_{50} for a constant void ratio can be also derived theoretically. A model of an assembly of elastic spheres and the contact theory of Hertz [21] and Mindlin [35] are used. For an identical external normal force N, the two assemblies of spheres with different diameters shown in Fig. 16a have the same stiffness both, in the axial direction and with respect to a shear loading. Of course the void ratio is also identical for both assemblies.

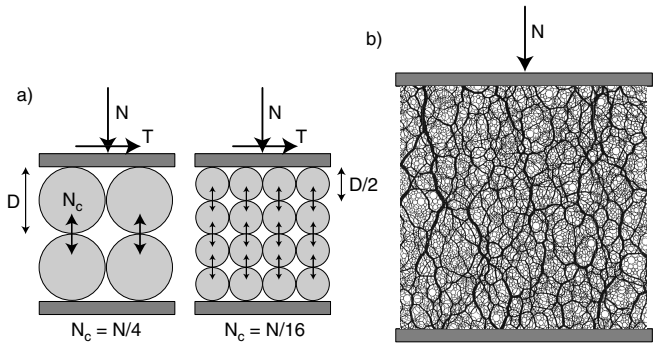

Fig. 16: a) Assemblies of $2 \times 2 \times 2$ and $4 \times 4 \times 4$ elastic spheres, b) Normal force chains in a polydisperse packing (line thickness is proportional to the normal force), results from numerical simulations performed by Radjai & Wolf [39]

A micromechanical explanation of the decrease of $G_{\max}$ with increasing coefficient of uniformity for a constant void ratio can be given comparing the force transmission chains in monodisperse and in polydisperse materials (Radjai & Wolf [39], Radjai et al. [40]). In a monodisperse material representing a uniformly composed sand (Fig. 16a), the force chains are rather equally distributed. In a polydisperse material representing a non-uniformly composed granular packing, strong and weak force chains are formed through the interparticle contacts (Fig. 16b). A contact is defined as "strong" if it transmits a normal force N_c greater than the average value N_c^{av} of all contacts. If $N_c < N_c^{\text{av}}$ applies, the contact is "weak". Numerical simulations of a polydisperse packing (Radjai & Wolf [39]) showed that the weak contacts transmit only approx. 28 % of the average mean pressure p in the granular packing. The shear forces T_c transmitted by the weak contacts are even negligibly small. Thus, a large portion of grains ("weak phase") are only marginally involved in the transmission of external shear forces but decrease void ratio since they occupy space in the grain skeleton. Considering an arbitrary horizontal section of a monodisperse assembly, the sum of normal contact forces in the "strong phase" chains is equal to the external load N. According to Radjai & Wolf [39], for a polydisperse assembly this value is only about $0.72N$. Considering a certain external shear strain γ applied to the monodisperse and the polydisperse assembly and taking into account the proportionality between normal stresses and shear stresses, a smaller shear stress will develop in the polydisperse packing. The lower shear stiffness of a polydisperse packing compared to a monodisperse one is in good accordance with the experimental findings of the present study.

The concept of "skeleton void ratio" used for example by Polito & Martin [37] in order to describe the influence of the fines content FC may be also adapted. In a binary packing of large and small grains, below a "limiting fines content" (usually > 25 %) the small grains fill the voids between the large grains. Although they reduce the void ratio, the fine grains do not significantly influence the mechanical properties (e.g. $G_{\max}$) of the skeleton formed by the large grains. The "skeleton void ratio", defined as the void ratio that would exist in the packing if all fine particles were removed, has been reported to be more representative for the sand behavior at small FC-values (e.g. for the liquefaction resistance, Polito & Martin [37]). Although the clean sands with high C_u-values tested in the present study consist of various sizes of grains, the effect of the smaller grains may be quite similar to the role of the fines in the binary packing, that means they reduce the void ratio but do not significantly affect $G_{\max}$.

Summary, conclusions and outlook

163 resonant column tests have been performed on 25 different grain size distribution curves of a quartz sand. It has been demonstrated for a constant void ratio that in the investigated range (0.1 mm $\leq d_{50} \leq 6$ mm, $1.5 \leq C_u = d_{60}/d_{10} \leq 8$) the small-strain shear modulus $G_{\max}$ does not depend on the mean grain size d_{50}, but significantly decreases with increasing coefficient of uniformity C_u. Different correlations have been developed for $G_{\max}$ or for the modulus coefficient $K_{2,\max}$, respectively. The parameters A, a and n of the well-known Hardin's equation have been correlated with C_u. Using Hardin's equation and the proposed correlations $A, a, n(C_u)$, the $G_{\max}$-values of the tested grain size distribution curves are well predicted for different void ratios and pressures. A correlation of the modulus coefficient $K_{2,\max}$ with C_u has also been pro-

posed. Due to the fixed exponent $n = 0.5$ of the pressure-dependence, the prediction is slightly less accurate. If the data are presented in the form $G_{\max}(D_r)$ or $K_{2,\max}(D_r)$ with the relative density D_r, the scatter is quite significant. However, the proposed correlations in terms of relative density may be sufficiently accurate for practical purposes (i.e. for a rough estimation).

The proposed correlations predict quite well most of the $G_{\max}$-values reported in the literature for sands with a sub-angular grain shape. For round and angular grains, an extension of the proposed correlations considering the influence of the shape of the particles seems necessary. For the application of the proposed empirical formulas to in-situ conditions, suitable corrections of the laboratory data have been discussed. Furthermore, a micromechanical explanation of the experimental observations has been given.

The suitability of the proposed equations for "more complicated" grain size distribution curves has to be checked. Up to now only grain size distribution curves with a linear shape in the semi-logarithmic scale have been tested. S-shaped and gap-graded grain size distribution curves as well as more "naturally" shaped curves will be tested in future. The influence of the fines content is also being studied and will be integrated into the proposed correlations. Further tests will be conducted regarding the influence of the grain shape on the dependence $G_{\max}(C_u)$. The small-strain constrained elastic modulus $M_{\max}$, Poisson's ratio ν and the curves $G_{\sec}(\gamma)$ and $D(\gamma)$ in dependence of the grain size distribution curve will be discussed in separate papers in future.

Acknowledgements

The presented study has been performed within the framework of the project "Influence of the coefficient of uniformity of the grain size distribution curve and of the fines content on the dynamic properties of non-cohesive soils" funded by the German Research Council (DFG, project No. TR218/11-1). The authors are grateful to DFG for the financial support. The RC tests have been performed at Ruhr-University Bochum, Germany. The authors gratefully acknowledge the help of the diploma thesis students R. Martinez, F. Durán-Graeff, E. Giolo and M. Navarrete Hernández.

References

[1] *DIN 18126: Bestimmung der Dichte nichtbindiger Böden bei lockerster und dichtester Lagerung*, 1996.

[2] S.S. Afifi and Jr. Richart, F.E. Stress-history effects on shear modulus of soils. *Soils and Foundations*, 13(1):77–95, 1973.

[3] S.S. Afifi and R.D. Woods. Long-term pressure effects on shear modulus of soils. *Journal of the Soil Mechanics and Foundations Division, ASCE*, 97(SM10):1445–1460, 1971.

[4] A. Alarcon-Guzman, J.L. Chameau, G.A. Leonardos, and J.D. Frost. Shear modulus and cyclic undrained behavior of sands. *Soils and Foundations*, 29(4):105–119, 1989.

[5] A.S. Amat. Elastic stiffness moduli of Hostun Sand. Master's thesis, University of Bristol, 2007.

[6] C.D.P. Baxter. *An experimental study on the aging of sands*. PhD thesis, Faculty of the Virginia Polytechnic Institute and State University, July 1999.

[7] R. Bellotti, M. Jamiolkowski, D.C.F. Lo Presti, and D.A. O'Neill. Anisotropy of small strain stiffness in Ticino sand. *Géotechnique*, 46(1):115–131, 1996.

[8] G. Castro and S.J. Poulos. Factors affecting liquefaction and cyclic mobility. *Journal of the Geotechnical Engineering Division, ASCE*, 103(GT6):501–516, 1977.

[9] S.K. Chaudhary, J. Kuwano, and Y. Hayano. Measurement of quasi-elastic stiffness parameters of dense Toyoura sand in hollow cylinder apparatus and triaxial apparatus with bender elements. *Geotechnical Testing Journal, ASTM*, 27(1):23–35, 2004.

[10] R.M. Chung, F.Y. Yokel, and H. Wechsler. Pore pressure buildup in resonant column tests. *Journal of Geotechnical Engineering, ASCE*, 110(2):247–261, 1984.

[11] V.P. Drnevich and F.E. Richart. Dynamic prestraining of dry sand. *Journal of the Soil Mechanics and Foundations Division, ASCE*, 96(SM2):453–467, 1970.

[12] P.M. Duku, J.P. Stewart, D.H. Whang, and E. Yee. Volumetric strains of clean sands subject to cyclic loads. *Journal of Geotechnical and Geoenvironmental Engineering, ASCE*, 134(8):1073–1085, 2008.

[13] T.B. Edil and G.-F. Luh. Dynamic modulus and damping relationsships for sands. In *Proc. ASCE Spec. Conf. on Earthquake Engin. and Soil Dyn.*, volume 1, pages 394–409, 1978.

[14] V. Fioravante. Anisotropy of small strain stiffness of Ticino and Kenya sands from seismic wave propagation measured in triaxial testing. *Soils and Foundations*, 40(4):129–142, 2000.

[15] V. Fioravante and R. Capoferri. On the use of multi-directional piezoelectric transducers in triaxial testing. *Geotechnical Testing Journal, ASTM*, 24(3):243–255, 2001.

[16] G. Gazetas. *Foundation Engineering Handbook, 2nd Edition*, chapter 15: Foundation vibrations, pages 553–593. 1991.

[17] B.O. Hardin and W.L. Black. Sand stiffness under various triaxial stresses. *Journal of the Soil Mechanics and Foundations Division, ASCE*, 92(SM2):27–42, 1966.

[18] B.O. Hardin and M.E. Kalinski. Estimating the shear modulus of gravelly soils. *Journal of Geotechnical and Geoenvironmental Engineering, ASCE*, 131(7):867–875, 2005.

[19] B.O. Hardin and F.E. Richart Jr. Elastic wave velocities in granular soils. *Journal of the Soil Mechanics and Foundations Division, ASCE*, 89(SM1):33–65, 1963.

[20] Ch. Heiniger. Dynamic properties of sands and gravel based on resonant column tests (in German). *Geotechnik*, 8:76–81, 1985.

[21] H. Hertz. Über die Berührung fester elastischer Körper. *Journal reine und angewandte Mathematik*, 92:156–171, 1881.

[22] K. Ishihara. *Soil Behaviour in Earthquake Geotechnics*. Oxford Science Publications, 1995.

[23] T. Iwasaki and F. Tatsuoka. Effects of grain size and grading on dynamic shear moduli of sands. *Soils and Foundations*, 17(3):19–35, 1977.

[24] T. Iwasaki, F. Tatsuoka, and Y. Takagi. Shear moduli of sands under cyclic torsional shear loading. *Soils and Foundations*, 18(1):39–56, 1978.

[25] D.P. Knox, K.H.II Stokoe, and S.E. Kopperman. Effects of state of stress on velocity of low-amplitude shear wave propagating along principal stress directions in dry sand. Technical Report GR 82-23, University of Texas, Austin, 1982.

[26] T. Kokusho, T. Hara, and R. Hiraoka. Undrained shear strength of granular soils with different particle gradations. *Journal of Geotechnical and Geoenvironmental Engineering, ASCE*, 130(6):621–629, 2004.

[27] J. Koseki, S. Kawakami, H. Nagayama, and T. Sato. Change of small strain quasi-elastic deformation properties during undrained cyclic torsional shear and triaxial tests of Toyoura sand. *Soils and Foundations*, 40(3):101–110, 2000.

[28] P.V. Lade, C.D Liggio, and J.A. Yamamuro. Effects of non-plastic fines on minimum and maximum void ratios of sand. *Geotechnical Testing Journal, ASTM*, 21(4):336–347, 1998.

[29] K.L. Lee and J.A. Fitton. Factors affecting the cyclic loading strength of soil. In *Vibration Effects of Earthqakes on Soils and Foundations, ASTM Special Technical Publication 450*, pages 71–95, 1969.

[30] X.S. Li, W.L. Yang, C.K. Chen, and W.C. Wang. Energy-injecting virtual mass resonant column system. *Journal of Geotechnical and Geoenvironmental Engineering, ASCE*, 124(5):428–438, 1998.

[31] D.C.F. Lo Presti, O. Pallara, R. Lancellotta, M. Armandi, and R. Maniscalco. Monotonic and cyclic loading behaviour of two sands at small strains. *Geotechnical Testing Journal, ASTM*, (4):409–424, 1993.

[32] P.B. Lontou and C.P. Nikolopoulou. Effect of Grain Size on Dynamic Shear Modulus of Sands: An Experimental Investigation (in Greek). Dept. of Civil Engineering, University of Patras, Greece, July 2004.

[33] R. Martinez. Influence of the grain size distribution curve on the stiffness and the damping ratio of non-cohesive soils at small strains (in German). Diploma thesis, Institute of Soil Mechanics and Foundation Engineering, Ruhr-University Bochum, 2007.

[34] F.-Y. Menq and K.H. Stokoe II. Linear dynamic properties of sandy and gravelly soils from large-scale resonant tests. In Di Benedetto et al., editor, *Deformation Characteristics of Geomaterials*, pages 63–71. Swets & Zeitlinger, Lisse, 2003.

[35] R.D. Mindlin and H. Deresiewicz. Elastic spheres in contact under varying oblique forces. *Journal of Applied Mechanics*, 20:327–344, 1953.

[36] A. Niemunis, T. Wichtmann, and T. Triantafyllidis. A high-cycle accumulation model for sand. *Computers and Geotechnics*, 32(4):245–263, 2005.

[37] C. Polito and J. Martin. Effects of nonplastic fines on the liquefaction resistance of sands. *Journal of Geotechnical and Geoenvironmental Engineering, ASCE*, 127(5):408–415, 2001.

[38] X. Qian, D.H. Gray, and R.D. Woods. Voids and granulometry: effects on shear modulus of unsaturated sands. *Journal of Geotechnical Engineering, ASCE*, 119(2):295–314, 1993.

[39] F. Radjai and D.E. Wolf. Features of static pressure in dense granular media. *Granular Matter*, (1):3–8, 1998.

[40] F. Radjai, D.E. Wolf, M. Jean, and J.-J. Moreau. Bimodal character of stress transmission in granular packings. *Physical Review Lett.*, 80(1):61–64, 1998.

[41] S.K. Roesler. Anisotropic shear modulus due to stress anisotropy. *Journal of the Geotechnical Engineering Division, ASCE*, 105(GT7):871–880, 1979.

[42] K.M. Rollins, M.D. Evans, N.B. Diehl, and W.D. Daily III. Shear modulus and damping relationships for gravels. *Journal of Geotechnical and Geoenvironmental Engineering, ASCE*, 124(5):396–405, 1998.

[43] S.K. Saxena and K.R. Reddy. Dynamic moduli and damping ratios for Monterey No. 0 sand by resonant column tests. *Soils and Foundations*, 29(2):37–51, 1989.

[44] H.B. Seed and I.M. Idriss. Soil moduli and damping factors for dynamic response analyses. Technical Report EERC 70-10, Earthquake Engineering Research Center, University of California, Berkeley, 1970.

[45] H.B. Seed, R.T. Wong, I.M. Idriss, and K. Tokimatsu. Moduli and damping factors for dynamic analyses of cohesionless soil. *Journal of Geotechnical Engineering, ASCE*, 112(11):1016–1032, 1986.

[46] C.K. Shen, X.S. Li, and Y.Z. Gu. Microcomputer based free torsional vibration test. *Journal of Geotechnical Engineering, ASCE*, 111(8):971–986, 1985.

[47] F. Tatsuoka, T. Iwasaki, S. Yoshida, S. Fukushima, and H. Sudo. Shear modulus and damping by drained tests on clean sand specimen reconstituted by various methods. *Soils and Foundations*, 19(1):39–54, 1979.

[48] S. Teachavorasinskun, F. Tatsuoka, and D.C.F. Lo Presti. Effects of cyclic prestraining on dilatancy characteristics and liquefaction of sand. In Shibuya, Mitachi, and Miura, editors, *Pre-failure deformation of geomaterials*, pages 75–80, 1994.

[49] I. Towhata. *Geotechnical Earthquake Engineering*. Springer, 2008.

[50] Y.P. Vaid, J.M. Fisher, R.H. Kuerbis, and D. Negussey. Particle gradation and liquefaction. *Journal of Geotechnical Engineering, ASCE*, 116(4):698–703, 1990.

[51] T. Wichtmann. Explicit accumulation model for non-cohesive soils under cyclic loading. PhD thesis, Publications of the Institute of Soil Mechanics and Foundation Engineering, Ruhr-University Bochum, Issue No. 38, available from www.rz.uni-karlsruhe.de/∼gn97/, 2005.

[52] T. Wichtmann, A. Niemunis, and T. Triantafyllidis. Strain accumulation in sand due to cyclic loading: drained triaxial tests. *Soil Dynamics and Earthquake Engineering*, 25(12):967–979, 2005.

[53] T. Wichtmann, A. Niemunis, and T. Triantafyllidis. On the influence of the polarization and the shape of the strain loop on strain accumulation in sand under high-cyclic loading. *Soil Dynamics and Earthquake Engineering*, 27(1):14–28, 2007.

[54] T. Wichtmann and Th. Triantafyllidis. Influence of a cyclic and dynamic loading history on dynamic properties of dry sand, part I: cyclic and dynamic torsional prestraining. *Soil Dynamics and Earthquake Engineering*, 24(2):127–147, 2004.

[55] S. Wu, D.H. Gray, and F.E. Richart Jr. Capillary effects on dynamic modulus of sands and silts. *Journal of Geotechnical Engineering, ASCE*, 110(9):1188–1203, 1984.

[56] P. Yu and F.E. Richart Jr. Stress ratio effects on shear modulus of dry sands. *Journal of Geotechnical Engineering, ASCE*, 110(3):331–345, 1984.